THE JOURNAL OF PHYSICAL CHEMISTRY LETTERS
A JOURNAL OF THE AMERICAN CHEMICAL SOCIETY

pubs.acs.org/JPCL

Letter

Adatoms in the Surface-Confined Ullmann Coupling of Phenyl Groups

Zhenzhe Zhang, Dmitrii F. Perepichka,* and Rustam Z. Khaliullin*

Cite This: *J. Phys. Chem. Lett.* 2021, 12, 11061−11069

Read Online

ACCESS | Metrics & More | Article Recommendations | Supporting Information

ABSTRACT: Despite the importance of the on-surface Ullmann coupling for synthesis of atomically precise carbon nanostructures, it is still unclear whether this reaction is catalyzed by surface atoms or adatoms. Here, the feasibility of the adatom creation and adatom-catalyzed Ullmann coupling of chloro-, bromo-, and iodobenzene on Cu(111), Ag(111), and Au(111) surfaces is examined using density functional theory modeling. The extraction of a metal atom is found to be greatly facilitated by the formation of strong phenyl−metal bonds, making the extraction energy barrier comparable to, and in the case of Ag(111) even lower than, that for the competing surface-catalyzed phenyl−phenyl bond formation. However, if the phenyl−adatom bonds are too strong, as on Cu(111) and Ag(111), they create an insurmountable barrier for the subsequent adatom-catalyzed C−C coupling. In contrast, Au adatoms do not bind phenyl groups strongly and can catalyze the C−C bond formation almost as efficiently as surface atoms.

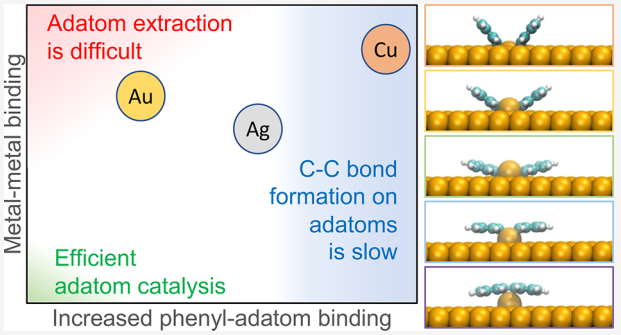

The unique and tunable properties of π-conjugated nanomaterials such as graphene nanoribbons[1−5] and two-dimensional conjugated organic polymers[6−16] make them promising candidates for a variety of electronic and optoelectronic devices. Practical applications of these materials in devices require scalable methods to create extended structures with low defect density. The Ullmann coupling of aryl halides on metal surfaces—copper, silver, and gold—is currently the most promising bottom-up strategy to assemble atomically precise π-conjugated carbon nanostructures with a high degree of control over their electronic properties.[2,7,17−26]

The mechanism of the surface-confined Ullmann coupling has been studied with a variety of experimental techniques including scanning tunneling microscopy (STM), atomic force microscopy (AFM), and temperature-programmed reaction spectroscopy.[27−37] Experimental investigation is often augmented by computer modeling crucial for interpreting ambiguous experimental data. It is widely accepted that aryl halide molecules physisorbed on a metal surface dissociate with the formation of surface-bound halogens and aryl groups.[27,35,38,39] The aryl intermediates diffuse on the surface and, once sufficiently close to each other, combine with the formation of an organometallic carbon−metal−carbon bridge structure. This intermediate undergoes reductive elimination to form a covalent carbon−carbon bond between the two aryls.

Although substantial progress has been made elucidating the mechanism of the Ullmann coupling, our knowledge of several details remains incomplete. Experimental data has been interpreted based almost exclusively on models that describe metal surfaces as ideal, perfectly ordered structures. Metal surfaces, however, are not free of defects. These defects range from three-dimensional defects such as pores[40] and cracks[41] to planar defects such as twin boundaries[42] and stacking faults,[43] line defects such as dislocations,[44] and to point defects such as adatoms[45] and vacancies.[46]

Although the equilibrium concentration of adatoms on metal surfaces is expected to be small[47,48]—on the order of 10^{-9} on Cu and Ag around room temperature[48]—due to the high energy of their formation,[49] such pre-existing adatoms have been known to form on copper, silver, and gold surfaces[50,51] near terrace edges and kinks.[52,53] These pre-existing adatoms have also been found to participate in metal organic coordination networks.[54−59] There is a growing body of evidence that adatoms can be created in the process of on-surface reactions.[24,49,59−63] Quantifying the extent to which adatoms and other imperfections of the metal surface influence the thermodynamics and kinetics of the Ullmann coupling can inform new strategies for reaction optimization, leading, in turn, to better defect-free assembly of two-dimensional polymers.

It has been recently suggested based on results of an STM and density functional theory (DFT) investigation of the on-

Received: September 4, 2021
Accepted: November 4, 2021
Published: November 8, 2021

https://doi.org/10.1021/acs.jpclett.1c02914
J. Phys. Chem. Lett. 2021, 12, 11061−11069

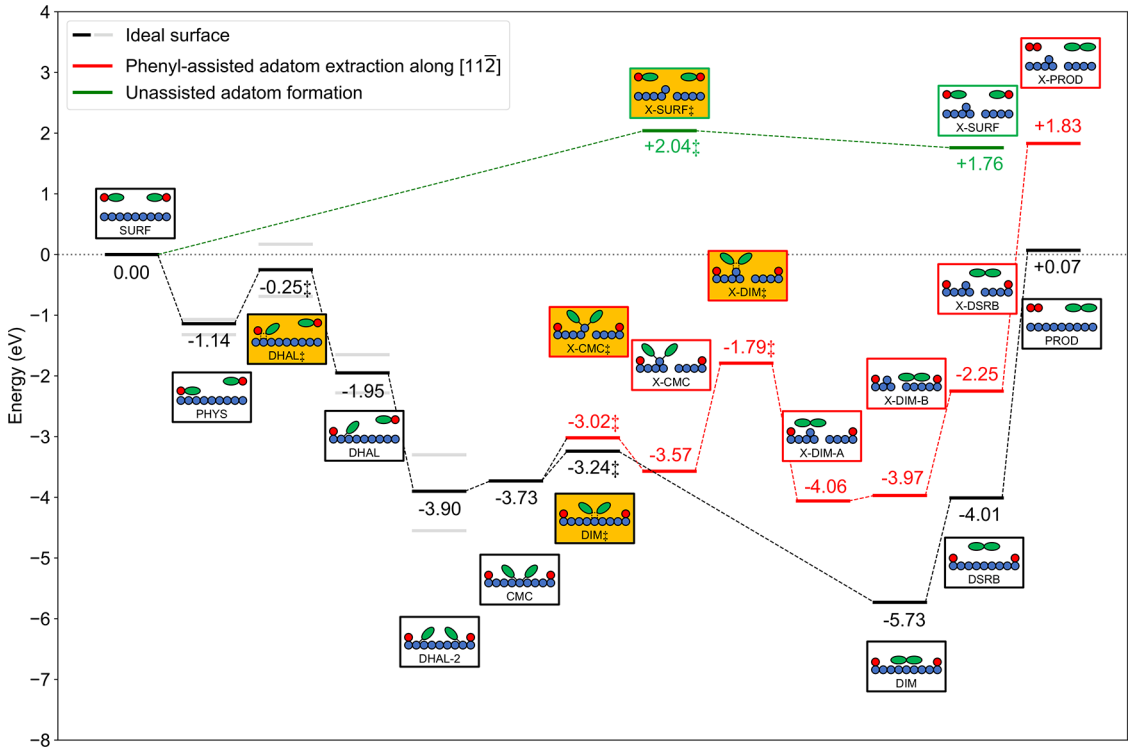

Figure 1. Energy profile of the Ullmann reaction of monohalogentated benzenes on Cu(111). In the pictograms, the yellow background marks transition states; blue, red, and green shapes denote copper atoms, halogen atoms, and phenyl groups, respectively. Energy levels shown with black are states with bromine as the halogen, whereas the gray upper and lower levels denote states with chlorine and iodine as the halogen, respectively. It is assumed that halogen atoms do not influence the reaction after the dehalogenation step (but see refs 70−72), and therefore, only the energy levels for bromine containing species are shown (see Tables S1, S3, and S4 for all numerical values). The following abbreviations are used to denote states. **SURF** surface and gas-phase molecules, **PHYS** one precursor molecule is physisorbed, **DHAL** one molecule is dehalogenated, **DHAL-2** two molecules are dehalogenated, **CMC** carbon−metal−carbon bridge intermediate, **DIM** biphenyl product, **X-DIM-A** biphenyl product adsorbed on adatom, **X-DIM-B** biphenyl product adsorbed on the surface, **DSRB** biphenyl is desorbed, **PROD** all products are desorbed. The **X** prefix in all abbreviations denotes an eXtracted adatom.

surface Ullmann coupling reaction that metals atoms bonded to one iodine and one phenyl fragments—the products of the dehalogenation of an iodobenzene molecule—can be lifted from their positions and placed on the surface, forming adatoms.[49] The energy required for this extraction has been calculated to be 0.88, 0.53, and 0.35 eV for Cu(111), Ag(111), and Au(111) surface—noticeably lower than the 1.71, 1.12 and 1.15 eV adatom formation energies on surfaces without organic species.[49] It has also been estimated that the reduced adatom extraction energy can be partially compensated by the release of energy in the preceding dehalogenation step.[49]

The role of adatoms has also been investigated for another step of the Ullmann coupling: the formation of carbon−metal−carbon bridge structures.[64−66] For example, DFT modeling shows that two fluoranthenyl groups lift their shared gold atom 2.2 Å above its ideal surface position, which is noticeably higher than the 0.5 Å height produced by a single group[65] and almost equal to the 2.8 Å interplanar spacing of Au(111) planes. The lifting of this magnitude suggests that aryl radicals can in principle shift the lifted atom laterally on the surface so it can no longer recombine with its vacancy. However, such a hypothetical aryl-assisted adatom creation has neither been demonstrated experimentally nor studied computationally.

In contrast, pre-existing adatoms have been considered in the case of the formation of the C−M−C bridge from two triphenylene groups on a Cu(111) surface. The 3.90(25) Å carbon−carbon distance measured using AFM has been found to agree more closely with the 3.86 Å distance calculated for a DFT model with an adatom acting as the bridge rather than with the 3.42 Å distance calculated for the structure with a highly lifted ideal surface atom.[64] The energy of the formation of the adatom-containing organometallic bridge has also been calculated to be 1.74 eV lower than the energy of the formation of the intermediate on the ideal surface.[64]

In a study of the C−M−C intermediates formed by two 4-bromoterphenyl groups on a Cu(111) surface, a comparison of the degree of molecular twisting in experimental and simulated AFM images has also indicated that it is an adatom that serves as the metal bridge.[66] Furthermore, an analysis of the ratio of the two types of organometallic C−M−C intermediates at different temperatures suggests that adatoms can be created during the reaction.[66]

Unfortunately, the role of adatoms in the formation of the carbon−carbon bond, the final key step of the on-surface Ullmann coupling, has not been investigated. Although the C−C bond formation on a gold atom lifted high above the surface has been studied computationally in the case of bromofluoranthene, the investigation focused exclusively on the pathway where the lifted atom returns to its original crystallographic position in the surface.[65] Despite the emerging evidence of adatoms being a part of some of the organometallic bridge structures,[64,66] it remains unclear whether surface atoms can be extracted by two organic groups. Moreover, it is unknown

https://doi.org/10.1021/acs.jpclett.1c02914
J. Phys. Chem. Lett. 2021, 12, 11061−11069

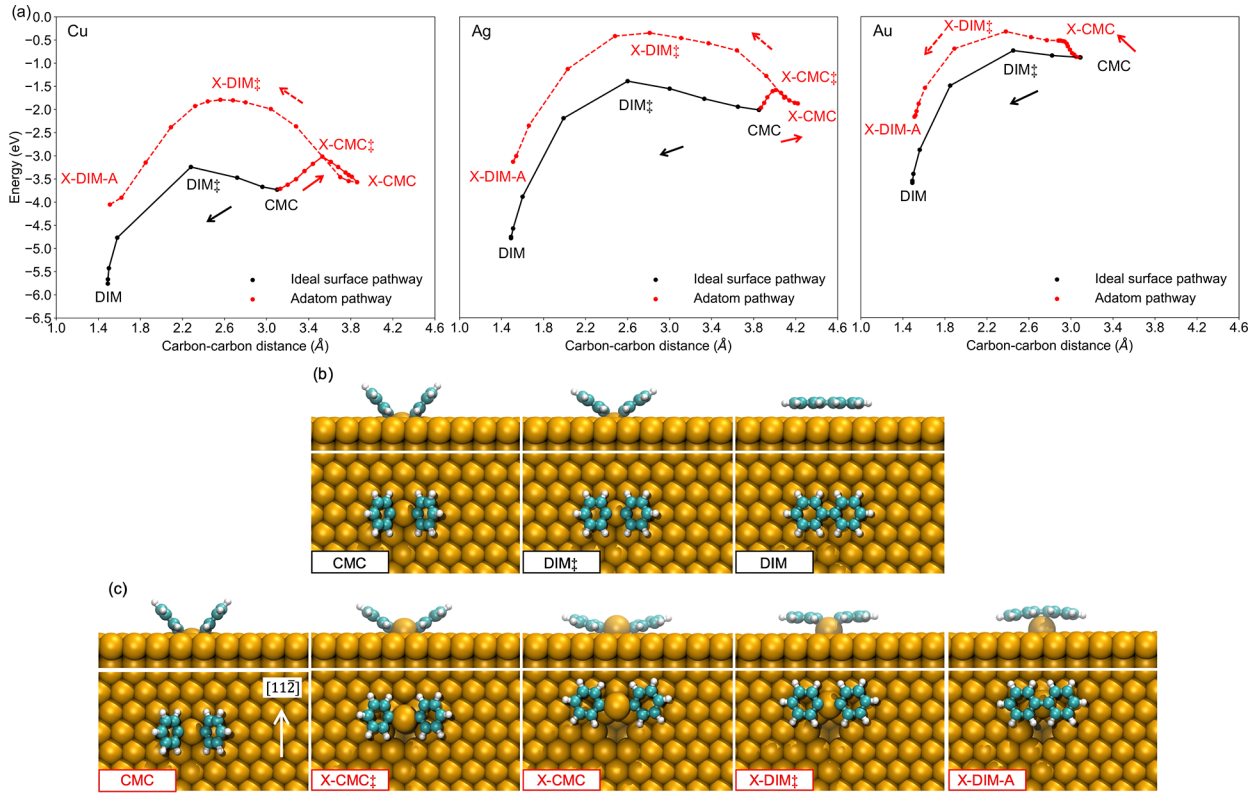

Figure 2. Coupling of the phenyl groups along the ideal-surface (black) and adatom (red) pathways. (a) Nudged elastic band (NEB) energy profiles along the reaction coordinate represented by the distance between the two carbon atoms. For the Cu(111) surface, the geometry of key intermediates is shown along the (b) ideal-surface and (c) adatom pathways.

whether the extracted adatoms can be left behind on the surface, uncoordinated to any groups, after the carbon−carbon bond is formed.

In order to answer these questions, this work examines, for the first time, the energetics of the adatom creation during the on-surface coupling of two phenyl groups using DFT modeling. Furthermore, previously unexplored effects of adatoms, extracted and pre-existing, on the carbon−carbon bond formation between two phenyl groups are investigated in detail. The phenyl group, which is produced in the dehalogenation of monosubstituted benzenes, is chosen in this work as the simplest and most studied representative of aromatic building blocks used in on-surface synthesis of carbon nanomaterials. The energetics of all steps of the Ullmann reaction is compared for three different metals (Cu, Ag, Au) and three halogens (Cl, Br, I) but the main focus of this work is on the formation of a C−C bond.

Slab models were employed to represent metal surfaces. DFT calculations were performed using the dispersion-corrected[67,68] Perdew−Burke−Ernzerhof[69] functional (see Computational Methods for details). The coupling reaction on the Cu(111) surface is discussed in detail first. Coupling on the Ag(111) and Au(111) surfaces is considered in comparison with the Cu(111) surface next.

Ullmann coupling on Cu(111). In the initial steps of the Ullmann reaction (Figure 1) the halogenated benzene molecules, physisorbed on the metal surface (**PHYS**), dissociate forming the surface-bound phenyl groups (**DHAL**), which then combine forming organometallic C−M−C bridge structures (**CMC**). The calculated energy profiles of these steps for three halogens (Figures 1 and S1−S3 and Table S1) are in qualitative agreement with the trends in the experimentally measured onset temperatures of dehalogenation (Table S2)[35,70,73] and with the previous calculations on this[32,74] and similar systems.

Two pathways to create the C−C bond are considered here. In the first pathway, the bridge Cu atom in **CMC** returns to its original position after the C−C bond is formed. This pathway is referred to as the ideal-surface pathway. In the second pathway, the Cu atom is pulled out to become an adatom, leaving a vacancy in its original position. This pathway is called the adatom pathway.

The C−C bond formation along the ideal-surface path is so exothermic (−2.00 eV) that it can be considered irreversible at the typical temperatures of the Ullmann coupling of phenyl groups on copper (350 K) .[27,73] The energies of the initial (**CMC**), transition (**DIM‡**) and final states (**DIM**, for biphenyl) along the ideal-surface pathway are shown in Figure 1 whereas their structures and the nudged elastic band (NEB) energy profile are presented in Figure 2. Figure 2 and Table S3 show that, in this pathway, the bridge cooper atom returns back to its position isochronously with the C−C bond formation. The ideal-surface path has a relatively small 0.49 eV energy barrier, in agreement with previous calculations (Table S3) .[74,75] It should be pointed out that the relative barrier heights for the dehalogenation and C−C bond formation steps calculated in this and previous works[74,75] are inconsistent with the experimentally measured onset temperatures (Table S2). Although the origin of this disagreement remains unclear (see the Supporting Information), the results of this work, which focuses on the C−C bond formation step, are not expected to be affected substantially.

https://doi.org/10.1021/acs.jpclett.1c02914
J. Phys. Chem. Lett. 2021, 12, 11061−11069

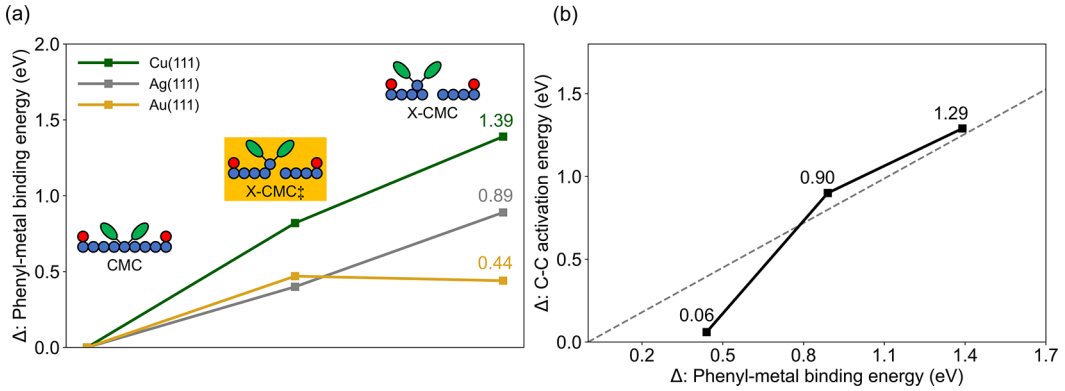

Figure 3. (a) Strength of the interaction energy between the two phenyl groups and the surface, measured as the change from the **CMC** state. (b) Dependence between the decreased catalytic activity of adatoms and strengthening of the phenyl-adatom binding. In both axis labels, Δ refers to the change from the ideal surface to adatom. The linear trendline enforced to go through the origin is $y = 0.898x$ ($R^2 = 0.950$).

The adatom pathway consists of three elementary steps: the adatom extraction with assistance of phenyls, the C−C bond formation on the adatom, and the diffusion of biphenyl away from the adatom.

Among several alternative adatom pathways (see Supporting Information), the extraction along the [11$\bar{2}$] high-symmetry surface direction (Figure 2) has the lowest energy barrier and will be considered further.

The barrier of the extraction of a Cu atom bonded to two phenyl groups (0.71 eV, **CMC** to **X-CMC**) is substantially lower than the 2.04 eV energy required to form an adatom without the assistance of phenyl groups (green pathway in Figure 1). The decreased barrier height is due to the stronger binding of the phenyl groups to the Cu adatom (Figure 3a, also note the 0.12 Å shortening of the carbon−metal bond from **CMC** to **X-CMC** in Table S4). Remarkably, the adatom extraction assisted by two phenyl groups requires less energy (0.16 eV) than the previously described extraction assisted by a single phenyl group and a halogen atom (0.88 eV) .[49]

With the permissive energetics of adatom extraction, it is important to look closely into the formation of the C−C bond catalyzed by the adatom. The energy released along this step (**X-CMC** to **X-DIM-A**) is moderate −0.48 eV (cf. − 2.00 eV on the ideal surface from **CMC** to **DIM**) while the barrier height (from **X-CMC** to **X-DIM‡**) is prohibitive 1.78 eV (cf. 0.49 eV i.e. **CMC** to **DIM‡**). This difference between the ideal-surface and adatom pathways can be attributed to the strong bonds between the phenyl groups and adatom. The cleavage of these bonds hinders the C−C bond formation as much as their formation facilitates the extraction step.

It is worth noting that the adatom pathway can also be viewed as a sum of two different steps: the exothermic ideal-surface C−C bond formation (−2.00 eV) and the energy-demanding unassisted adatom formation (1.76 eV). The entire pathway is, therefore, nearly thermoneutral (−0.24 eV). Interestingly, all three steps along the adatom pathway—extraction, C−C bond formation, and the biphenyl diffusion—are also almost thermoneutral and have their own energy balancing mechanisms (Figure 1). In the first step, the adatom escapes the pull of its metal neighbors with the compensating strengthening of the two phenyl−adatom bonds. In the second step, the two strong carbon−adatom bonds are converted into one equally strong C−C bond, without a significant release of energy. Finally, the biphenyl drifts away from the adatom without experiencing a strong resisting force. Despite the permissive thermodynamics, however, the high energy of the state renders the biphenyl formation through the adatom pathway unlikely. Moreover, despite the ease of the phenyl-assisted adatom extraction, the organometallic bridges containing extracted adatoms (**X-CMC**) are unlikely to be observed in STM or AFM experiments. This is because the competing C−C bond formation on the ideal surface has a low barrier and produces the equilibrium mixture heavily dominated by biphenyl molecules (**DIM**).

Coupling on Pre-existing Cu Adatoms. We also examined the Ullmann coupling catalyzed by the adatoms that are not extracted during the reaction but already exist on the Cu(111) surface. Such pre-existing adatoms are known to form on Cu surfaces due to thermal fluctuations around various defects such as terrace edges and kinks.[48]

Figure 4 shows the strong synergistic binding of two phenyl groups to a pre-existing Cu adatom. While the first phenyl is

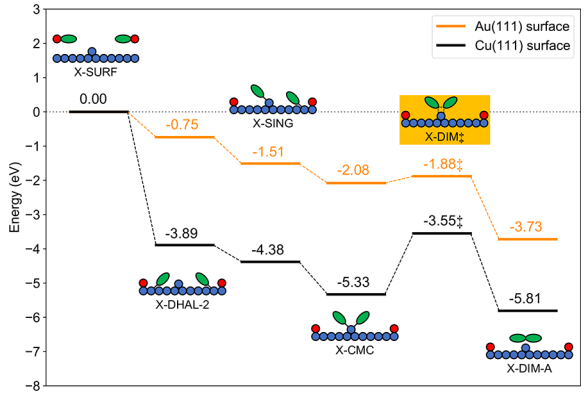

Figure 4. Energy profiles of the Ullmann reaction of bromobenzene on pre-existing adatoms on Cu(111) and Au(111) surfaces.

coordinated to a Cu adatom with the energy release of 0.49 eV (**X-DHAL-2** to **X-SING**), binding of the second phenyl is accompanied by the release of additional 0.95 eV (**X-SING** to **X-CMC**). On Cu(111), the system system becomes trapped in the **X-CMC** state. On one hand, the C−C bond formation cannot proceed because of the height of the **X-DIM‡** barrier (1.78 eV). On the other hand, the reverse dissociation of the strong adatom−phenyl bond also requires at least 0.95 eV of energy. Because of such **X-CMC** traps, the presence of adatoms during the Ullmann polymerization on Cu(111)

https://doi.org/10.1021/acs.jpclett.1c02914
J. Phys. Chem. Lett. 2021, 12, 11061−11069

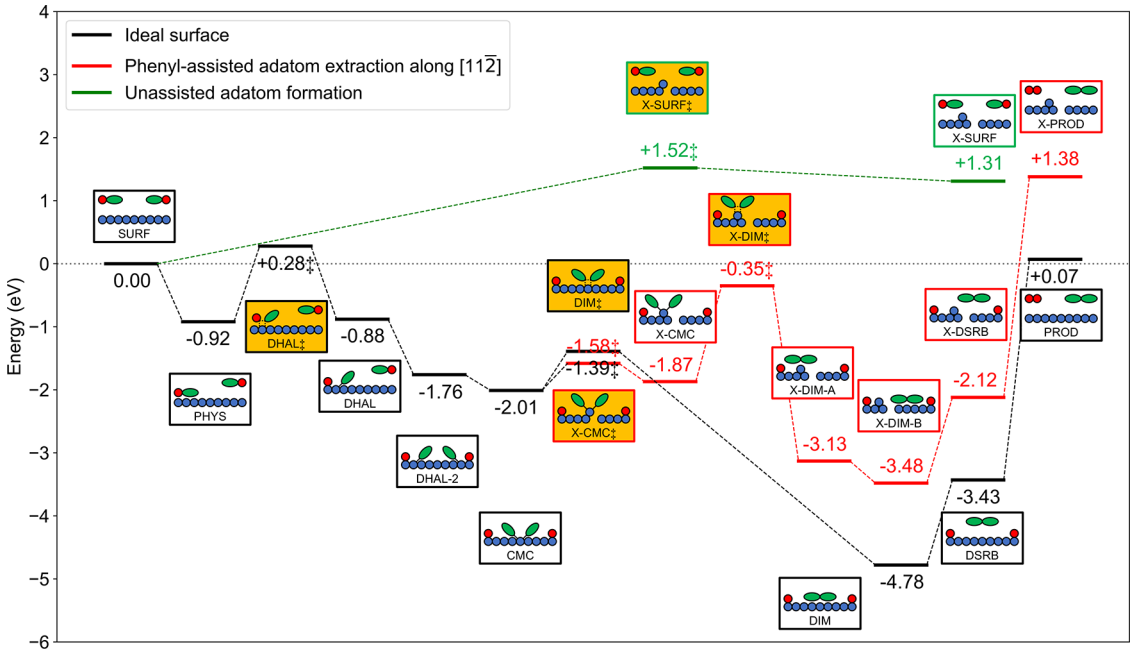

Figure 5. Energy profile of the Ullmann reaction of bromobenzene on Ag(111). Color coding and abbreviations are the same as in Figure 1.

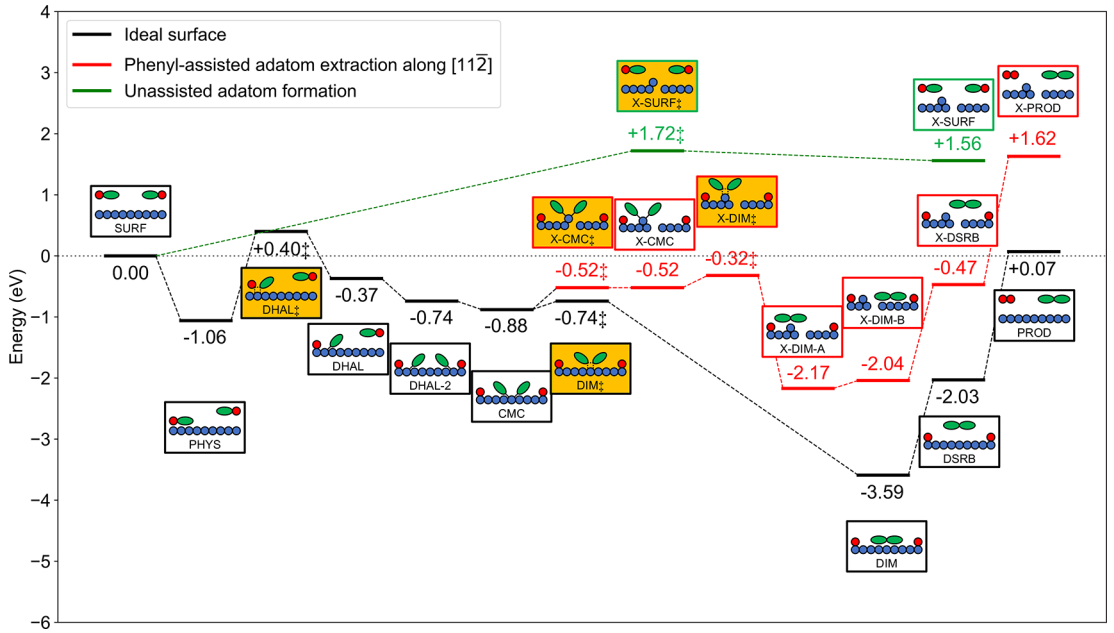

Figure 6. Energy profile of the Ullmann reaction of bromobenzene on Au(111). Color coding and abbreviations are the same as in Figure 1.

surface is more likely to lead to defects in assembled nanostructures than to be the dominant mechanism of the Ullmann coupling.

Ullmann Reaction on Ag(111) and Au(111). Energy profiles of the Ullmann reaction on the ideal Ag(111) and Au(111) surfaces were calculated for bromobenzene (Figures 5 and 6). The energy barriers of the debromination step (i.e., formation of **DHAL**) increase from Cu (0.89 eV) to Ag (1.20 eV) and to Au (1.46 eV) in agreement with the trend in the experimentally measured dehalogenation temperatures[35,70,73] (Table S2) and with previous calculations.[74] At the same time, the energy barriers of the C−C formation step (**CMC** to **DIM‡**, Figure 2a, Table S3) follow a different trend decreasing from Ag (0.62 eV) to Cu (0.49 eV) and to Au (0.14 eV), again in agreement with experimental (Table S2) and previously reported DFT[74] trends. The adatom pathways on Ag(111) and Au(111) exhibit several interesting features not seen for Cu(111).

First, the phenyl-assisted adatom extraction on Ag(111) surface has a lower activation energy (0.43 eV from **CMC** to **X-CMC‡**) and thus proceeds faster than the conventional ideal-surface C−C bond formation (0.62 eV from **CMC** to **DIM‡**), in contrast to the Cu-mediated processes (Figure 2a). However, despite the fast formation of the phenyl-bonded adatoms on Ag(111), the fate of these species is the same as those on Cu(111): silver adatoms quickly recombine with their vacancies and the biphenyl formation occurs along the conventional ideal-surface pathway, which has a lower

https://doi.org/10.1021/acs.jpclett.1c02914
J. Phys. Chem. Lett. 2021, 12, 11061−11069

activation barrier (0.62 eV from **CMC** to **DIM‡**) than that of adatom-catalyzed coupling (1.52 eV from **X-CMC** to **X-DIM‡**).

Second, the barrier of the adatom-catalyzed C−C formation on Au (0.20 eV **X-CMC** to **X-DIM‡**, Figure 6) is dramatically lower than those for Ag (1.52 eV) and Cu (1.78 eV) (Figure 2a). However, when the additional 0.36 eV barrier of the Au atom extraction is taken into account, it is clear that the transformation along the adatom pathway is significantly slower than the rapid C−C bond formation on the ideal surface with its 0.14 eV activation energy. Since the extraction barrier is eliminated for pre-existing Au adatoms, they are expected to catalyze the C−C bond formation almost as efficiently as ideal-surface atoms, without forming the **X-CMC** traps like Cu adatoms[76] (Figure 4).

To summarize, the calculations show that adatoms on all three surfaces have decreased ability to catalyze the C−C bond formation compared to metal atoms of the ideal surfaces. The key reason behind the decreased catalytic activity is the strengthening of the phenyl-metal binding as demonstrated by the nearly linear dependence between the two properties in Figure 3b.

Implications for Adatom Catalysis. The results of this work raise a tantalizing question whether it is at all possible to find a metal surface capable of catalyzing the Ullmann coupling through an adatom pathway that is faster than the conventional ideal-surface mechanism. The DFT data reveals that the strengthening of the phenyl−adatom binding relative to the phenyl-surface binding (Figure 3) is the main parameter that determines the efficiency of both the extraction and adatom-catalyzed C−C bond formation steps (Figure 3b). The example of Au(111) demonstrates that low strengthening leads to weak extraction assistance. On the other hand, the examples of Ag(111) and Cu(111) show that high strengthening may facilitate the extraction but prohibits the second C−C bond formation step. It is reasonable to expect, however, that the phenyl-assisted extraction can be facilitated without hindering the adatom catalyzed C−C bond formation if metal catalysts with lower energy of unassisted adatom extraction are employed. It can be speculated that alloys of copper, silver, and gold with different ratios of components can satisfy this requirement because lattice inequalities may make atom extraction easier.

To conclude, the role of adatoms in the coupling of iodo-, bromo-, and chlorobenzene on Cu(111), Ag(111), and Au(111) surfaces was investigated using DFT modeling. For all three metals, the energy of the phenyl-assisted adatom extraction was found to be significantly lower than the energy of the unassisted adatom creation. In the most dramatic example, Cu(111), the two energies are 0.16 and 1.76 eV, respectively. In the case of the phenyl-assisted metal atom extraction, the energy cost of breaking metal−metal bonds is almost completely offset by the increased binding of the phenyl groups to the extracted metal atom. This effect is also responsible for the low phenyl-assisted extraction barriers computed for all three metals (0.71 eV Cu, 0.43 eV Ag, 0.36 eV Au).

Quantifying the strengthening of phenyl−adatom bonds for all three metals revealed its strong correlation with the increased activation barrier of the C−C bond formation on adatoms. In the case of Cu(111) and Ag(111), the adatom-catalyzed C−C bond formation barriers are found to be extremely high (1.78 eV Cu, 1.52 eV Ag) rendering this adatom-based catalytic mechanism uncompetitive despite the ease of the phenyl-assisted adatom extraction. In stark contrast to Cu and Ag, the C−C bond formation barrier on Au adatoms is only 0.20 eV. Nevertheless, the adatom catalysis on Au is still slower than the ideal-surface catalysis because it is the extraction step that hinders it in this case.

DFT is used to predict the behavior of not only the phenyl-extracted adatoms but also the adatoms that already exist on metal surfaces, for example, around steps and kinks. On Cu(111) and Ag(111), pre-existing adatoms bind phenyl groups so strongly that they are unable to catalyze the subsequent C−C bond formation. Without the possibility to recombine with a vacancy, these organometallic adatom states form low-energy traps. In contrast, pre-existing Au adatoms are not expected to form such traps as they catalyze the C−C bond formation almost as efficiently as ideal-surface atoms. This may explain why the Ullmann polymerization on Au(111) can produce fewer defects in surface-assembled nanostructures than the same process on Ag(111) and Cu(111) .[76]

This work has important implications. The systematic comparison of the reaction energetics on ideal surfaces and adatoms allows rational predictions to be made about the influence of other defects, such as terrace edges and kinks, on the Ullmann coupling reactions, facilitating investigation of their mechanisms. The systematic DFT data can also advance design of effective adatom catalysts for a variety of on-surface reactions. One strategy to design adatom catalyzed reactions is to focus on metals with low adatom-vacancy formation energies while a complementary strategy would be to find reactants that bind to adatoms and surface atoms equally strongly.

COMPUTATIONAL METHODS

The (111) metal surfaces were modeled with slabs containing 192 metal atoms arranged in four 8 × 6 atomic layers. A 10 Å portion of vacuum was added in the direction normal to the surface to ensure weak interaction between periodic images of the slab. The size of the slabs in the lateral directions was 20.55 × 13.35 Å for Cu, 22.84 × 14.82 Å for Ag, and 22.47 × 14.60 Å for Au. When pre-existing atoms are considered, it is assumed that the presence of the vacancy does not affect the state energetics drastically and, therefore, the vacancy-containing models are reused to model pre-existing adatoms.

DFT calculations were performed using the Vienna *ab initio* simulation package (VASP) .[77−80] The dispersion-corrected[67,68] Perdew−Burke−Ernzerhof (PBE) generalized gradient approximation[69] was used as the exchange-correlation functional. Spin-polarized electronic states were modeled using a plane wave basis set with the energy cutoff set at 800 eV. The projector augmented wave formalism was used to describe interactions of atomic cores with valence electrons. The integration over the Brillouin zone was performed using the 3 × 3 × 1 Monkhorst−Pack *k*-point mesh.

Atomic positions were optimized until the maximum force on atoms decreased below 0.02 eV Å^{-1}. Transition state structures were located using the climbing-image nudged elastic band (NEB) with the VTST code.[81] In NEB calculations, an improved initial guess[82,83] for the minimum energy path was used, and the positions of atoms were relaxed until the maximum force dropped below 0.1 eV Å^{-1}.

The role of entropy in the on-surface reactions was investigated using the model of mobile rigid adsorbates[84] described in the Supporting Information. Figures S6 and S7

https://doi.org/10.1021/acs.jpclett.1c02914
J. Phys. Chem. Lett. 2021, 12, 11061−11069

show that for commonly used experimental conditions (i.e., temperature and surface coverage), the entropy effects do not play a significant role in all adatom extraction and C−C bond formation elementary steps considered in this work.

■ ASSOCIATED CONTENT

Supporting Information

The Supporting Information is available free of charge at https://pubs.acs.org/doi/10.1021/acs.jpclett.1c02914.

> Formation of organometallic intermediates on Cu(111); characterization of the intermediates in the dehalogenation step on Cu(111); minimum experimentally measured temperatures necessary for the completion of the Ullmann coupling steps; comparison of the dehalogenation and C−C bond formation energy barriers; characterization of the intermediates in the C−C bond formation step along the ideal-surface and two adatoms pathways; alternative adatom pathways on Cu(111); approximate calculation of the free energy profiles (PDF)

■ AUTHOR INFORMATION

Corresponding Authors

Dmitrii F. Perepichka − *Department of Chemistry, McGill University, Montreal, QC H3A 0B8, Canada;* orcid.org/0000-0003-2233-416X; Email: dmitrii.perepichka@mcgill.ca

Rustam Z. Khaliullin − *Department of Chemistry, McGill University, Montreal, QC H3A 0B8, Canada;* orcid.org/0000-0002-9073-6753; Email: rustam.khaliullin@mcgill.ca

Author

Zhenzhe Zhang − *Department of Chemistry, McGill University, Montreal, QC H3A 0B8, Canada*

Complete contact information is available at: https://pubs.acs.org/10.1021/acs.jpclett.1c02914

Notes

The authors declare no competing financial interest.

■ ACKNOWLEDGMENTS

The research was funded by the Natural Sciences and Engineering Research Council of Canada (NSERC) through Discovery Grant (RGPIN-2016-0505) and by Triagency Institutional Programs Secretariat through New Frontiers in Research Fund (NFRFE-2018-00852). The authors are grateful for computer resources allocated under the CFI John R. Evans Leaders Fund program.

■ REFERENCES

(1) Cai, J.; Ruffieux, P.; Jaafar, R.; Bieri, M.; Braun, T.; Blankenburg, S.; Muoth, M.; Seitsonen, A. P.; Saleh, M.; Feng, X.; et al. Atomically Precise Bottom-Up Fabrication of Graphene Nanoribbons. *Nature* **2010**, *466*, 470−473.

(2) Talirz, L.; Ruffieux, P.; Fasel, R. On-Surface Synthesis of Atomically Precise Graphene Nanoribbons. *Adv. Mater.* **2016**, *28*, 6222−6231.

(3) Ruffieux, P.; Wang, S.; Yang, B.; Sánchez-Sánchez, C.; Liu, J.; Dienel, T.; Talirz, L.; Shinde, P.; Pignedoli, C. A.; Passerone, D.; et al. On-Surface Synthesis of Graphene Nanoribbons with Zigzag Edge Topology. *Nature* **2016**, *531*, 489−492.

(4) Zhang, H.; Lin, H.; Sun, K.; Chen, L.; Zagranyarski, Y.; Aghdassi, N.; Duhm, S.; Li, Q.; Zhong, D.; Li, Y.; et al. On-Surface Synthesis of Rylene-Type Graphene Nanoribbons. *J. Am. Chem. Soc.* **2015**, *137*, 4022−4025.

(5) Zhang, W.; Wang, Q.; Chen, Y.; Wang, Z.; Wee, A. T. S. Van der Waals stacked 2D layered materials for optoelectronics. *2D Mater.* **2016**, *3*, 022001.

(6) Grill, L.; Dyer, M.; Lafferentz, L.; Persson, M.; Peters, M.; Hecht, S. Nano-architectures by covalent assembly of molecular building blocks. *Nat. Nanotechnol.* **2007**, *2*, 687−691.

(7) Galeotti, G.; De Marchi, F.; Hamzehpoor, E.; MacLean, O. D.; Rajeswara Rao, M.; Chen, Y.; Besteiro, L. V.; Dettmann, D.; Ferrari, L.; Frezza, F.; et al. Synthesis of Mesoscale Ordered Two-Dimensional π-Conjugated Polymers with Semiconducting Properties. *Nat. Mater.* **2020**, *19*, 874−880.

(8) Cardenas, L.; Gutzler, R.; Lipton-Duffin, J.; Fu, C.; Brusso, J. L.; Dinca, L. E.; Vondráček, M.; Fagot-Revurat, Y.; Malterre, D.; Rosei, F.; et al. Synthesis and electronic structure of a two dimensional π-conjugated polythiophene. *Chem. Sci.* **2013**, *4*, 3263−3268.

(9) Grossmann, L.; King, B.; Reichlmaier, S.; Hartmann, N.; Rosén, J.; Heckl, W.; Björk, J.; Lackinger, M. On-surface photopolymerization of two-dimensional polymers ordered on the mesoscale. *Nat. Chem.* **2021**, *13*, 730−736.

(10) Xu, K.; Urgel, J. I.; Eimre, K.; Di Giovannantonio, M.; Keerthi, A.; Komber, H.; Wang, S.; Narita, A.; Berger, R.; Ruffieux, P.; et al. On-Surface Synthesis of a Nonplanar Porous Nanographene. *J. Am. Chem. Soc.* **2019**, *141*, 7726−7730.

(11) Chen, Y.; Zhang, X.; Yu, P.; Ma, Y. Stable dispersions of graphene and highly conducting graphene films: a new approach to creating colloids of graphene monolayers. *Chem. Commun.* **2009**, 4527−4529.

(12) Bai, H.; Xu, Y.; Zhao, L.; Li, C.; Shi, G. Non-covalent functionalization of graphene sheets by sulfonated polyaniline. *Chem. Commun.* **2009**, 1667−1669.

(13) Luo, J.; Cote, L. J.; Tung, V. C.; Tan, A. T. L.; Goins, P. E.; Wu, J.; Huang, J. Graphene Oxide Nanocolloids. *J. Am. Chem. Soc.* **2010**, *132*, 17667−17669.

(14) Wang, H.; Robinson, J. T.; Diankov, G.; Dai, H. Nanocrystal Growth on Graphene with Various Degrees of Oxidation. *J. Am. Chem. Soc.* **2010**, *132*, 3270−3271.

(15) Bhardwaj, T.; Antic, A.; Pavan, B.; Barone, V.; Fahlman, B. D. Enhanced Electrochemical Lithium Storage by Graphene Nanoribbons. *J. Am. Chem. Soc.* **2010**, *132*, 12556−12558.

(16) Du, A.; Zhu, Z.; Smith, S. C. Multifunctional Porous Graphene for Nanoelectronics and Hydrogen Storage: New Properties Revealed by First Principle Calculations. *J. Am. Chem. Soc.* **2010**, *132*, 2876−2877.

(17) Lackinger, M. Surface-Assisted Ullmann Coupling. *Chem. Commun.* **2017**, *53*, 7872−7885.

(18) Dong, L.; Liu, P. N.; Lin, N. Surface-Activated Coupling Reactions Confined on a Surface. *Acc. Chem. Res.* **2015**, *48*, 2765−2774.

(19) Sun, Q.; Zhang, R.; Qiu, J.; Liu, R.; Xu, W. On-Surface Synthesis of Carbon Nanostructures. *Adv. Mater.* **2018**, *30*, 1705630.

(20) De Marchi, F.; Galeotti, G.; Simenas, M.; Tornau, E. E.; Pezzella, A.; MacLeod, J.; Ebrahimi, M.; Rosei, F. Room-Temperature Surface-Assisted Reactivity of a Melanin Precursor: Silver Metal−Organic Coordination versus Covalent Dimerization on Gold. *Nanoscale* **2018**, *10*, 16721−16729.

(21) Zhong, D.; Franke, J.-H.; Podiyanachari, S. K.; Blömker, T.; Zhang, H.; Kehr, G.; Erker, G.; Fuchs, H.; Chi, L. Linear Alkane Polymerization on a Gold Surface. *Science* **2011**, *334*, 213−216.

(22) Di Giovannantonio, M.; Contini, G. Reversibility and Intermediate Steps as Key Tools for the Growth of Extended Ordered Polymers *via* On-Surface Synthesis. *J. Phys.: Condens. Matter* **2018**, *30*, 093001.

(23) Cui, D.; Perepichka, D. F.; MacLeod, J. M.; Rosei, F. Surface-Confined Single-Layer Covalent Organic Frameworks: Design, Synthesis and Application. *Chem. Soc. Rev.* **2020**, *49*, 2020−2038.

(24) Galeotti, G.; Di Giovannantonio, M.; Cupo, A.; Xing, S.; Lipton-Duffin, J.; Ebrahimi, M.; Vasseur, G.; Kierren, B.; Fagot-

Revurat, Y.; Tristant, D.; et al. An Unexpected Organometallic Intermediate in Surface-Confined Ullmann Coupling. *Nanoscale* **2019**, *11*, 7682−7689.
(25) Di Giovannantonio, M.; Tomellini, M.; Lipton-Duffin, J.; Galeotti, G.; Ebrahimi, M.; Cossaro, A.; Verdini, A.; Kharche, N.; Meunier, V.; Vasseur, G.; et al. Mechanistic Picture and Kinetic Analysis of Surface-Confined Ullmann Polymerization. *J. Am. Chem. Soc.* **2016**, *138*, 16696−16702.
(26) Vasseur, G.; Fagot-Revurat, Y.; Sicot, M.; Kierren, B.; Moreau, L.; Malterre, D.; Cardenas, L.; Galeotti, G.; Lipton-Duffin, J.; Rosei, F.; et al. Quasi One-Dimensional Band Dispersion and Surface Metallization in Long-Range Ordered Polymeric Wires. *Nat. Commun.* **2016**, *7*, 10235.
(27) Xi, M.; Bent, B. E. Iodobenzene on Cu(111): Formation and Coupling of Adsorbed Phenyl Groups. *Surf. Sci.* **1992**, *278*, 19−32.
(28) Han, P.; Mantooth, B. A.; Sykes, E. C. H.; Donhauser, Z. J.; Weiss, P. S. Benzene on Au(111) at 4K:Monolayer Growth and Tip -InducedMolecular Cascades.J. *J. Am. Chem. Soc.* **2004**, *126*, 10787−10793.
(29) Dameron, A. A.; Charles, L. F.; Weiss, P. S. Structures and Displacement of 1-Adamantanethiol Self-Assembled Monolayers on Au111. *J. Am. Chem. Soc.* **2005**, *127*, 8697−8704.
(30) Hla, S.-W.; Bartels, L.; Meyer, G.; Rieder, K.-H. Inducing All Steps of a Chemical Reaction with the Scanning Tunneling Microscope Tip: Towards Single Molecule Engineering. *Phys. Rev. Lett.* **2000**, *85*, 2777−2780.
(31) Zhou, X.; White, J. M. Photon- and Electron-Induced Chemistry of Chlorobenzene on Ag(111). *J. Chem. Phys.* **1990**, *92*, 5612−5621.
(32) Lipton-Duffin, J. A.; Ivasenko, O.; Perepichka, D. F.; Rosei, F. Synthesis of Polyphenylene Molecular Wires by Surface-Confined Polymerization. *Small* **2009**, *5*, 592−597.
(33) Gutzler, R.; Cardenas, L.; Lipton-Duffin, J.; El Garah, M.; Dinca, L. E.; Szakacs, C. E.; Fu, C.; Gallagher, M.; Vondráček, M.; Rybachuk, M.; et al. Ullmann-Type Coupling of Brominated Tetrathienoanthracene on Copper and Silver. *Nanoscale* **2014**, *6*, 2660−2668.
(34) Chen, M.; Xiao, J.; Steinrück, H.-P.; Wang, S.; Wang, W.; Lin, N.; Hieringer, W.; Gottfried, J. M. Combined Photoemission and Scanning Tunneling Microscopy Study of the Surface-Assisted Ullmann Coupling Reaction. *J. Phys. Chem. C* **2014**, *118*, 6820−6830.
(35) Xi, M.; Bent, B. E. Mechanisms of the Ullmann Coupling Reaction in Adsorbed Monolayers. *J. Am. Chem. Soc.* **1993**, *115*, 7426−7433.
(36) Szulczewski, G.; White, J. Thermal and Photon-Stimulated Reactions of Iodobenzene on Ag(111). *Surf. Sci.* **1998**, *399*, 305−315.
(37) Hla, S.-W.; Meyer, G.; Rieder, K.-H. Selective Bond Breaking of Single Iodobenzene Molecules with a Scanning Tunneling Microscope Tip. *Chem. Phys. Lett.* **2003**, *370*, 431−436.
(38) Song, Y.; Gardner, P.; Conrad, H.; Bradshaw, A.; White, J. A HREELS study of the UV photon-induced chemistry of C_6H_5Cl adsorbed on Ag{111. *Surf. Sci.* **1991**, *248*, L279−L284.
(39) Syomin, D.; Koel, B. E. Adsorption of Iodobenzene (C_6H_5I) on Au(111) Surfaces and Production of Biphenyl ($C_6H_5−C_6H_5$). *Surf. Sci.* **2001**, *490*, 265−273.
(40) Li, J.; Fang, Q.; Liu, B.; Liu, Y. The Effects of Pore and Second-Phase Particle on the Mechanical Properties of Machining Copper Matrix from Molecular Dynamic Simulation. *Appl. Surf. Sci.* **2016**, *384*, 419−431.
(41) Zhong, Y.; Markmann, J.; Jin, H.-J.; Ivanisenko, Y.; Kurmanaeva, L.; Weissmüller, J. Crack Mitigation during Dealloying of $Au_{25}Cu_{75}$. *Adv. Eng. Mater.* **2014**, *16*, 389−398.
(42) Hu, F.; Abeyweera, S. C.; Yu, J.; Zhang, D.; Wang, Y.; Yan, Q.; Sun, Y. Quantifying Electrocatalytic Reduction of CO_2 on Twin Boundaries. *Chem.* **2020**, *6*, 3007−3021.
(43) Dupraz, M.; Beutier, G.; Rodney, D.; Mordehai, D.; Verdier, M. Signature of Dislocations and Stacking Faults of Face-Centred Cubic Nanocrystals in Coherent X-Ray Diffraction Patterns: a Numerical Study. *J. Appl. Crystallogr.* **2015**, *48*, 621−644.
(44) Hu, Z.; Wu, Z.; Han, C.; He, J.; Ni, Z.; Chen, W. Two-Dimensional Transition Metal Dichalcogenides: Interface and Defect Engineering. *Chem. Soc. Rev.* **2018**, *47*, 3100−3128.
(45) Kotri, A.; El koraychy, E.; Mazroui, M.; Boughaleb, Y. Static Investigation of Adsorption and Hetero-Diffusion of Copper, Silver, and Gold Adatoms on the (111) Surface. *Surf. Interface Anal.* **2017**, *49*, 705−711.
(46) Torrelles, X.; Pensa, E.; Cortés, E.; Salvarezza, R.; Carro, P.; Hernández Guerrero, C.; Ocal, C.; Barrena, E.; Ferrer, S. Solving the Long-Standing Controversy of Long-Chain Alkanethiols Surface Structure on Au(111). *J. Phys. Chem. C* **2018**, *122*, 3893−3902.
(47) Lin, N.; Payer, D.; Dmitriev, A.; Strunskus, T.; Wöll, C.; Barth, J. V.; Kern, K. Two-Dimensional Adatom Gas Bestowing Dynamic Heterogeneity on Surfaces. *Angew. Chem., Int. Ed.* **2005**, *44*, 1488−1491.
(48) Giesen, M. Step and island dynamics at solid/vacuum and solid/liquid interfaces. *Prog. Surf. Sci.* **2001**, *68*, 1−154.
(49) Barton, D.; Gao, H.-Y.; Held, P. A.; Studer, A.; Fuchs, H.; Doltsinis, N. L.; Neugebauer, J. Formation of Organometallic Intermediate States in On-Surface Ullmann Couplings. *Chem. - Eur. J.* **2017**, *23*, 6190−6197.
(50) Bebensee, F.; Svane, K.; Bombis, C.; Masini, F.; Klyatskaya, S.; Besenbacher, F.; Ruben, M.; Hammer, B.; Linderoth, T. R. A Surface Coordination Network Based on Copper Adatom Trimers. *Angew. Chem., Int. Ed.* **2014**, *53*, 12955−12959.
(51) Dubois, M.-A.; Guillermet, O.; Gauthier, S.; Zhan, G.; Makoudi, Y.; Palmino, F.; Bouju, X.; Rochefort, A. Influence of Cu Adatoms on the Molecular Assembly of 4,4'-Bipyridine on Cu(111). *Phys. Chem. Chem. Phys.* **2018**, *20*, 15350−15357.
(52) Limot, L.; Pehlke, E.; Kröger, J.; Berndt, R. Surface-State Localization at Adatoms. *Phys. Rev. Lett.* **2005**, *94*, 036805.
(53) Voznyy, O.; Dubowski, J. J.; Yates, J. T.; Maksymovych, P. The Role of Gold Adatoms and Stereochemistry in Self-Assembly of Methylthiolate on Au(111). *J. Am. Chem. Soc.* **2009**, *131*, 12989−12993.
(54) Fan, Q.; Wang, C.; Han, Y.; Zhu, J.; Kuttner, J.; Hilt, G.; Gottfried, J. M. Surface-Assisted Formation, Assembly, and Dynamics of Planar Organometallic Macrocycles and Zigzag Shaped Polymer Chains with C−Cu−C Bonds. *ACS Nano* **2014**, *8*, 709−718.
(55) Sirtl, T.; Schlögl, S.; Rastgoo-Lahrood, A.; Jelic, J.; Neogi, S.; Schmittel, M.; Heckl, W. M.; Reuter, K.; Lackinger, M. Control of Intermolecular Bonds by Deposition Rates at Room Temperature: Hydrogen Bonds Versus Metal Coordination in Trinitrile Monolayers. *J. Am. Chem. Soc.* **2013**, *135*, 691−695.
(56) Walch, H.; Dienstmaier, J.; Eder, G.; Gutzler, R.; Schlögl, S.; Sirtl, T.; Das, K.; Schmittel, M.; Lackinger, M. Extended Two-Dimensional Metal−Organic Frameworks Based on Thiolate−Copper Coordination Bonds. *J. Am. Chem. Soc.* **2011**, *133*, 7909−7915.
(57) Pawin, G.; Wong, K.; Kim, D.; Sun, D.; Bartels, L.; Hong, S.; Rahman, T.; Carp, R.; Marsella, M. A Surface Coordination Network Based on Substrate-Derived Metal Adatoms with Local Charge Excess. *Angew. Chem., Int. Ed.* **2008**, *47*, 8442−8445.
(58) Kawai, S.; Sadeghi, A.; Okamoto, T.; Mitsui, C.; Pawlak, R.; Meier, T.; Takeya, J.; Goedecker, S.; Meyer, E. Organometallic Bonding in an Ullmann-Type On-Surface Chemical Reaction Studied by High-Resolution Atomic Force Microscopy. *Small* **2016**, *12*, 5303−5311.
(59) Judd, C.; Junqueira, F.; Haddow, S.; Champness, N.; Duncan, D.; Jones, R.; Saywell, A. Structural Characterisation of Molecular Conformation and the Incorporation of Adatoms in an On-Surface Ullmann-Type Reaction. *Commun. Chem.* **2020**, *3*, 166.
(60) Fan, Q.; Liu, L.; Dai, J.; Wang, T.; Ju, H.; Zhao, J.; Kuttner, J.; Hilt, G.; Gottfried, J. M.; Zhu, J. Surface Adatom Mediated Structural Transformation in Bromoarene Monolayers: Precursor Phases in Surface Ullmann Reaction. *ACS Nano* **2018**, *12*, 2267−2274.
(61) Hu, J.; Hu, J.; Zhang, Z.; Shen, K.; Liang, Z.; Zhang, H.; Tian, Q.; Wang, P.; Jiang, Z.; Huang, H.; et al. Ullmann Coupling of 2,7-Dibromopyrene on Au(111) Assisted by Surface Adatoms. *Appl. Surf. Sci.* **2020**, *513*, 145797.

https://doi.org/10.1021/acs.jpclett.1c02914
J. Phys. Chem. Lett. 2021, 12, 11061−11069

(62) Moreno-López, J. C.; Mowbray, D. J.; Pérez Paz, A.; de Campos Ferreira, R. C.; Ceccatto dos Santos, A.; Ayala, P.; de Siervo, A. Roles of Precursor Conformation and Adatoms in Ullmann Coupling: An Inverted Porphyrin on Cu(111). *Chem. Mater.* **2019**, *31*, 3009−3017.
(63) Eichhorn, J.; Strunskus, T.; Rastgoo-Lahrood, A.; Samanta, D.; Schmittel, M.; Lackinger, M. On-Surface Ullmann Polymerization via Intermediate Organometallic Networks on Ag(111). *Chem. Commun.* **2014**, *50*, 7680−7682.
(64) Zint, S.; Ebeling, D.; Schlöder, T.; Ahles, S.; Mollenhauer, D.; Wegner, H. A.; Schirmeisen, A. Imaging Successive Intermediate States of the On-Surface Ullmann Reaction on Cu(111): Role of the Metal Coordination. *ACS Nano* **2017**, *11*, 4183−4190.
(65) Nagoya, A.; Tetsuka, H.; Ohba, N. Mechanisms of Covalent Coupling Reaction of Dibromofluoranthene on Au(111). *J. Phys. Chem. C* **2018**, *122*, 17756−17763.
(66) Ebeling, D.; Zhong, Q.; Schlöder, T.; Tschakert, J.; Henkel, P.; Ahles, S.; Chi, L.; Mollenhauer, D.; Wegner, H. A.; Schirmeisen, A. Adsorption Structure of Mono- and Diradicals on a Cu(111) Surface: Chemoselective Dehalogenation of 4-Bromo-3"-Iodo-P-Terphenyl. *ACS Nano* **2019**, *13*, 324−336.
(67) Grimme, S.; Antony, J.; Ehrlich, S.; Krieg, H. A Consistent and Accurate *Ab Initio* Parametrization of Density Functional Dispersion Correction (DFT-D) for the 94 Elements H-Pu. *J. Chem. Phys.* **2010**, *132*, 154104.
(68) Grimme, S.; Ehrlich, S.; Goerigk, L. Effect of the Damping Function in Dispersion Corrected Density Functional Theory. *J. Comput. Chem.* **2011**, *32*, 1456−1465.
(69) Perdew, J. P.; Burke, K.; Ernzerhof, M. Generalized Gradient Approximation Made Simple. *Phys. Rev. Lett.* **1996**, *77*, 3865−3868.
(70) Galeotti, G.; Di Giovannantonio, M.; Lipton-Duffin, J.; Ebrahimi, M.; Tebi, S.; Verdini, A.; Floreano, L.; Fagot-Revurat, Y.; Perepichka, D. F.; Rosei, F.; et al. The Role of Halogens in On-Surface Ullmann Polymerization. *Faraday Discuss.* **2017**, *204*, 453−469.
(71) Peyrot, D.; Silly, F. On-Surface Synthesis of Two-Dimensional Covalent Organic Structures versus Halogen-Bonded Self-Assembly: Competing Formation of Organic Nanoarchitectures. *ACS Nano* **2016**, *10*, 5490−5498.
(72) Di Giovannantonio, M.; Deniz, O.; Urgel, J. I.; Widmer, R.; Dienel, T.; Stolz, S.; Sánchez-Sánchez, C.; Muntwiler, M.; Dumslaff, T.; Berger, R.; et al. On-Surface Growth Dynamics of Graphene Nanoribbons: The Role of Halogen Functionalization. *ACS Nano* **2018**, *12*, 74−81.
(73) Lewis, E. A.; Murphy, C. J.; Liriano, M. L.; Sykes, E. C. H. Atomic-Scale Insight into the Formation, Mobility and Reaction of Ullmann Coupling Intermediates. *Chem. Commun.* **2014**, *50*, 1006−1008.
(74) Björk, J.; Hanke, F.; Stafström, S. Mechanisms of Halogen-Based Covalent Self-Assembly on Metal Surfaces. *J. Am. Chem. Soc.* **2013**, *135*, 5768−5775.
(75) Nguyen, M.-T.; Pignedoli, C. A.; Passerone, D. An *Ab Initio* Insight into the Cu(111)-Mediated Ullmann Reaction. *Phys. Chem. Chem. Phys.* **2011**, *13*, 154−160.
(76) Bieri, M.; Nguyen, M.-T.; Gröning, O.; Cai, J.; Treier, M.; Aït-Mansour, K.; Ruffieux, P.; Pignedoli, C. A.; Passerone, D.; Kastler, M.; et al. Two-Dimensional Polymer Formation on Surfaces: Insight into the Roles of Precursor Mobility and Reactivity. *J. Am. Chem. Soc.* **2010**, *132*, 16669−16676.
(77) Kresse, G.; Hafner, J. *Ab Initio* Molecular Dynamics for Liquid Metals. *Phys. Rev. B: Condens. Matter Mater. Phys.* **1993**, *47*, 558−561.
(78) Kresse, G.; Hafner, J. *Ab Initio* Molecular-Dynamics Simulation of the Liquid-Metal−Amorphous-Semiconductor Transition in Germanium. *Phys. Rev. B: Condens. Matter Mater. Phys.* **1994**, *49*, 14251−14269.
(79) Kresse, G.; Furthmüller, J. Efficiency of *Ab-Initio* Total Energy Calculations for Metals and Semiconductors Using a Plane-Wave Basis Set. *Comput. Mater. Sci.* **1996**, *6*, 15−50.
(80) Kresse, G.; Furthmüller, J. Efficient Iterative Schemes for *Ab Initio* Total-Energy Calculations Using a Plane-Wave Basis Set. *Phys. Rev. B: Condens. Matter Mater. Phys.* **1996**, *54*, 11169−11186.
(81) Henkelman, G.; Uberuaga, B. P.; Jónsson, H. A Climbing Image Nudged Elastic Band Method for Finding Saddle Points and Minimum Energy Paths. *J. Chem. Phys.* **2000**, *113*, 9901−9904.
(82) Smidstrup, S.; Pedersen, A.; Stokbro, K.; Jónsson, H. Improved Initial Guess for Minimum Energy Path Calculations. *J. Chem. Phys.* **2014**, *140*, 214106.
(83) Henkelman, G.; Jónsson, H. Improved Tangent Estimate in the Nudged Elastic Band Method for Finding Minimum Energy Paths and Saddle Points. *J. Chem. Phys.* **2000**, *113*, 9978−9985.
(84) Hill, T. *An Introduction to Statistical Thermodynamics; Addison-Wesley series in chemistry*; Dover Publications, 1986.

https://doi.org/10.1021/acs.jpclett.1c02914
J. Phys. Chem. Lett. 2021, 12, 11061−11069